Improved depth resolution in near-infrared diffuse reflectance spectroscopy using obliquely oriented fibers

Rachel Estelle Thilwind
Gert 't Hooft
Natallia E. Uzunbajakava
Philips Research
High Tech Campus 34
5656 AE Eindhoven
The Netherlands

Abstract. We demonstrate a significant improvement of depth selectivity when using obliquely oriented fibers for near-infrared (NIR) diffuse reflectance spectroscopy. This is confirmed by diffuse reflectance measurements of a two-layer tissue-mimicking phantom across the spectral range from 1000 to 1940 nm. The experimental proof is supported by Monte Carlo simulations. The results reveal up to fourfold reduction in the mean optical penetration depth, twofold reduction in its variation, and a decrease in the number of scattering events when a single fiber is oriented at an angle of 60 deg. The effect of reducing the mean optical penetration depth is enhanced by orienting both fibers inwardly. Using outwardly oriented fibers enables more selective probing of deeper layers, while reducing the contribution from surface layers. We further demonstrate that the effect of an inward oblique arrangement can be approximated to a decrease in fiber-to-fiber separation in the case of a perpendicular fiber arrangement. This approximation is valid in the weak- or absorption-free regime. Our results assert the advantages of using obliquely oriented fibers when attempting to specifically address superficial tissue layers, for example, for skin cancer detection, or in noninvasive glucose monitoring. Such flexibility could be further advantageous in a range of minimally invasive applications, including catheter-based interventions.
 [DOI: 10.1117/1.3103339]

Keywords: diffuse reflectance; near-infrared (NIR) spectroscopy; Monte Carlo simulations; oblique orientation; depth selectivity; penetration depth.

Paper 08395R received Nov. 6, 2008; revised manuscript received Jan. 28, 2009; accepted for publication Jan. 28, 2009; published online Mar. 24, 2009.

1 Introduction

The method of using diffuse reflected light to measure optical properties of bulk tissue samples has been extensively described in the literature, e.g., by Wilson.[1] Although efforts have been made to refine diffuse optical techniques, depth selectivity, which impacts the sensitivity and specificity of the measurement, still remains a topic of debate in the literature.

The distinctive reflectance spectra yielded by the intra- and extracellular structures of the tissue and their relative distributions in superficial layers can be partially masked by multiply scattered light returning from deeper layers. This is especially the case if only the epidermis, with a typical thickness of less than 100 μm, is studied, e.g., for the purpose of diagnosing precancerous skin lesions.

A traditional solution is to experiment with the geometry of the probing interface. If more than one optical fiber is used, i.e., one for illumination and the other for collection of light (see Fig. 1), then the separation between the two fibers plays a significant role in the selectivity of the measurement: a larger separation will result in spectra being obtained from deeper layers in the tissue, while smaller separations will yield reflectance from the superficial layers.[1]

However, the depth selectivity of this approach for probing very shallow layers is still limited. Since the two fibers have a finite minimum separation distance, with this method, it is not possible to probe very shallow tissue layers, e.g., the epidermis, without some contribution from the layers below, e.g., the dermis.

Based on a similar principle, but showing far more potential for depth-selective probing, is the concept of oblique fiber orientation. In this technique, fiber separation distance is complemented by an additional variable: the angle of orientation of a fiber relative to the plane of the tissue surface. By varying the angle of orientation of one or both fibers (see Fig. 1), the result is a change in the average trajectory of the detected photon. Hence, the depth to which tissue is probed can be controlled accordingly.

The basis of the oblique orientation principle has been described and verified experimentally,[2–6] where it was used for deriving the optical properties of tissue. An optical design for Raman spectroscopy utilizing a non-normal angle to the surface of the sample reported on high selectivity of the probing

Address all correspondence to Rachel Thilwind, Care and Health Applications, Philips Research, High Tech Campus 34—Eindhoven, Noord-Brabant 5656AE Netherlands; Tel: 31402747816; Fax: 3140276321; E-mail: rachel.thilwind@philips.com

1083-3668/2009/14(2)/024026/9/$25.00 © 2009 SPIE

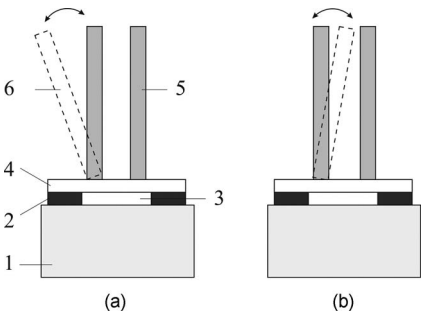

Fig. 1 Schematic diagram of an oblique illumination fiber concept and a multilayer phantom: (a) inward tilt; (b) outward tilt. Perpendicularly and obliquely oriented fibers are drawn using solid and dashed lines, respectively. 1—epoxy-based phantom layer; 2—spacer ring; 3—Intralipid layer contained in the spacer ring; 4—cover glass; 5—perpendicular-oriented fiber; and 6—obliquely oriented fiber.

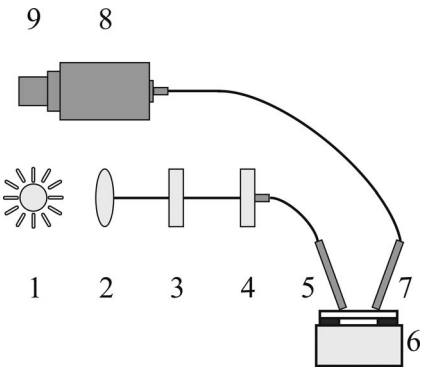

Fig. 2 Schematic diagram of the setup for measurements of diffuse reflectance. 1—light source; 2—collimating lens; 3—long-pass filter; 4—fiber coupler with SMA connector: 5, 7—illumination and collection fibers, respectively; 6—two-layer phantom; 8—monochromator; and 9—InGaAs photodetector array.

volume induced by varying the fiber angle.[7–9] Utzinger and Richards-Kortum performed a detailed investigation of fiber-optic probe designs for medical applications.[10] A number of studies were devoted to evaluating the performance of fluorescence spectroscopy as a function of illumination angle:[11–13] the angled illumination probe provided the capability to measure tissue fluorescence selectively from different depths within epithelial tissues.

Hattery et al.[14] reported on the influence of fiber angle in diffuse reflectance spectroscopy when measuring epithelial thickness in the visible wavelength range. Wang et al.[15] demonstrated that in the case of one inwardly obliquely oriented fiber [see Fig. 1(a)], the overlap of the illumination and collection cones constitutes a volume, the axial position of which differs compared to the case when two parallel fibers are used. An increase in the angle with respect to the plane of the tissue surface effectively confines light to a volume proximal to the surface. The converse also holds, in that an outwardly obliquely oriented fiber [see Fig. 1(b)] will on average result in longer photon trajectories and less reflected light will be collected from superficial layers. The impact of this effect is a higher signal-to-noise ratio in measurements where a tissue volume directly below the surface is selectively probed. This principle has been applied to skin cancer detection.[16,17]

Here, we focus on the application of the concept of obliquely positioned fibers in near-infrared (NIR) diffuse reflectance spectroscopy—a technique often used for a number of medical applications.[18–22] By combining experimental work on diffuse back-reflectance measurements in the broad spectral range from 1000 to 1940 nm with Monte Carlo simulations, we investigate the change in the absorption band scattering in diffuse back-reflectance spectra, the change in the mean penetration depth, and its variation as a function of fiber angle. Our investigation addresses both inward and outward obliquely oriented fiber arrangements.

We further compare an arrangement with a fixed fiber-to-fiber separation distance to a perpendicular-oriented arrangement with varying fiber-to-fiber separation, thereby assessing whether the effect of using an inward oblique arrangement can be approximated to a decrease of fiber-to-fiber separation distance in a perpendicular fiber arrangement.

Experiments were performed with the setup described in Fig. 2, and the results were compared with theoretical data yielded by Monte Carlo simulations, as detailed in Sec. 4.2.

2 Experimental Design

2.1 *Sample Preparation*

To verify the concept of oblique fibers, a two-layer tissue-mimicking phantom was constructed for use in the experiments. The phantom consisted of a 5-cm-thick solid epoxy-based scattering phantom layer underneath a volume of Intralipid solution of controlled thickness. A 20% Intralipid solution (Sigma) was diluted to a final concentration of 2% w/v. The optical properties of Intralipid and the epoxy-based phantom were obtained by measuring reflectance and transmittance using a spectrometer with an integrating sphere and applying the inverse adding-doubling (IAD) method to calculate the absorption and scattering coefficients. The measurement procedure and the IAD method have also been described in the literature.[23]

The absorption properties of Intralipid are dominated by water, for which the most intense spectral bands are located around 1199 nm, 1439 nm, and 1932 nm. The absorption coefficient of Intralipid and the epoxy-based phantom are given in Figs. 3(a) and 3(b), respectively. The most prominent spectral bands of the epoxy-based material can be seen around 1190 nm, 1140 nm, 1392 nm, 1432 nm, 1476 nm, 1546 nm, 1677 nm, 1697 nm, 1721 nm, and 1916 nm. The strongest spectral features—those around 1190 nm, 1140 nm, and 1721 nm—are used here as specific signatures of the epoxy-based phantom.

The reduced scattering coefficients of the Intralipid solution and the epoxy-based phantom were on the order of 1 mm^{-1}, respectively, showing a typical wavelength dependency.

The two-layer phantom was assembled in the following way. A 125-micrometer-thick metal ring was positioned on the solid epoxy-based phantom and was filled with Intralipid solution. A coverslip (22×22 mm, 130 to 160 μm thick, Esco) was put on top of the metal ring to ensure that the Intralipid layer was of a constant thickness. Optical contact

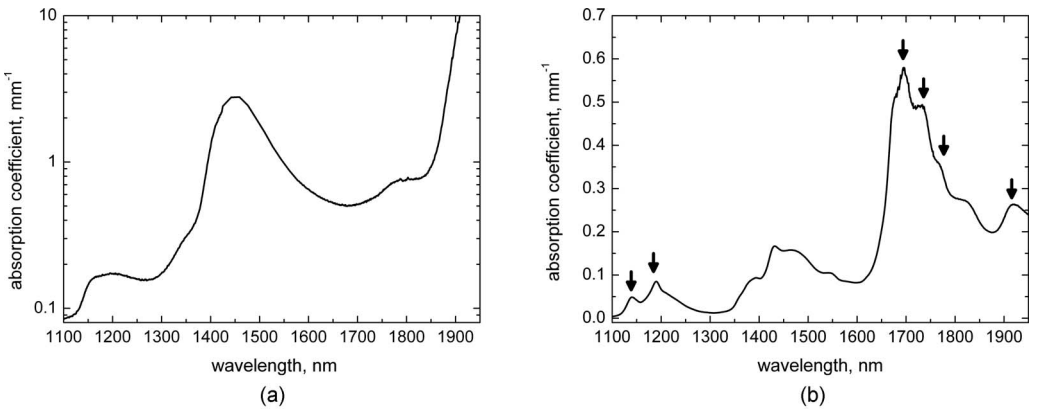

Fig. 3 Absorption coefficients of materials composing a two-layer phantom: (a) epoxy-based layer; (b) 2% w/v Intralipid solution. The absorption properties of Intralipid are dominated by water, where the most intense spectral bands are located around 1199 nm, 1439 nm, and 1932 nm. The most prominent spectral bands of the epoxy-based material can be seen around 1190 nm, 1140 nm, 1392 nm, 1432 nm, 1476 nm, 1546 nm, 1677 nm, 1697 nm, 1721 nm, and 1916 nm. The most strong spectral features of the epoxy-based material around 1190 nm, 1140 nm, and around 1721 nm are marked with arrows and will be used through this article as the specific signature of the epoxy-based phantom.

between the illumination and the collection fibers was improved by using a drop of carbo-fluoride-based immersion fluid (FC-40, $n=1.29$), which is optically transparent in the near-infrared (NIR) spectral region, although it should be noted that the use of immersion fluid does not eliminate reflectance at interfaces between the glass-Intralipid and Intralipid-epoxy layer (Intralipid $n=1.45$, glass=1.5, epoxy=1.56). Figure 1 shows a schematic diagram of the assembled two-layer phantom with the optical fibers.

2.2 *Experimental Setup*

A specialized unit for use in diffuse reflectance measurements of tissue (see Fig. 1) consisted of a sample stage, above which two optical fibers were mounted at a controlled height and center-to-center separation distance via microadjustment screws and a stepper motor. The fiber mounting unit setup was capable of maintaining a specific angular orientation of both optical fibers. Optical fibers of 600-micrometer core diameter were used in the experiment (Avantes BV). The center-to-center distance including the cladding was 820 μm.

All measurements with the oblique fiber unit were performed using an NIR spectrometer, which included a stabilized halogen lamp source, a monochromator (SpectraPro-150, Acton Research Corporation), and a liquid nitrogen–cooled InGaAs detector (OMA V:1024-2.2, Princeton Instruments; see Fig. 2). The diffraction grating of the spectrometer provided dispersion of 37.69 nm/mm, which covers 965 nm spectral range on the detector. A long-pass filter with a cutoff wavelength of 1000 nm was used in the illumination path to reject wavelengths below 1000 nm and to prevent overlap of higher diffraction orders on the light detector.

2.3 *Data Acquisition and Processing*

The optical spectra of the two-layer phantom were acquired and processed in the following way. First, the background signal was measured with no sample in place and no light falling on the detector: the main components of the background noise are thermal noise of the detector and thermal radiation from the environment. A signal was recorded during 20 ms with 2000 accumulations. This was followed by acquiring the spectrum of the light source back-reflected from a reflectance standard (Labsphere, certified reflectance standard).

Each acquired spectrum was subsequently corrected for the spectrally dependent setup throughput using the previously acquired spectrum of the light source. Wavelength calibration, i.e., a spatial relation between the detector pixels and a particular wavelength, was made by measuring the first and the second diffraction orders of HeNe laser and the diffuse back-reflectance spectrum of polystyrene, which is typically used for this purpose.[24]

3 Monte Carlo Design

All Monte Carlo simulations described here were performed using an experimentally validated routine based on code described in the literature,[25] which was extended by including the option of single oblique fiber orientation. To characterize light penetration in the phantom, we derived the mean penetration depth and the variation of mean penetration depth [see Eqs. (1) and (2)].

The mean penetration depth of a photon is defined as

$$\bar{Z}=\int_{entry}^{exit} z\cdot p(z)\mathrm{d}z=\sum_{i=0}^{n}\int_{p_i}^{p_{i+1}} z\cdot p(z)\mathrm{d}z=\sum_{i=0}^{n}\frac{zdpl}{L}, \quad (1)$$

where z is a level occupied by a photon along z, $p(z)$ is a probability of occupying a certain z level by a photon, L is the total photon path, and dpl is the differential photon pathlength.

The variation of mean penetration depth for a single photon is given by

$$std(Z)=(\overline{Z^2}-\bar{Z}^2)^{1/2}. \quad (2)$$

To avoid the typically long computation times of the current Monte Carlo simulation program, the original high-resolution spectra containing the optical properties of the epoxy-based solid phantom and Intralipid were resampled at a lower frequency. Namely, 40 data points for the whole spectral region

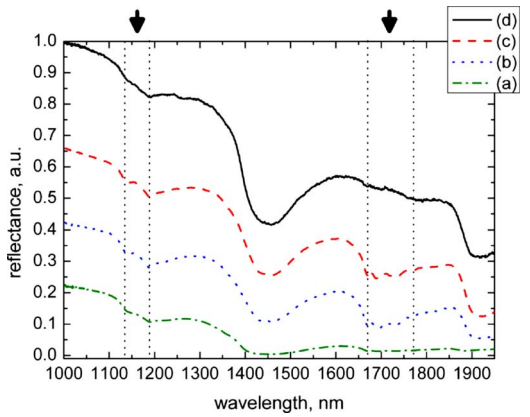

Fig. 4 Dependence of diffuse back-reflectance spectra of a two-layer phantom on the inward tilt of the illumination fiber. The angle of the illumination fiber was (a) 0 deg; (b) 20 deg; (c) 40 deg; and (d) 60 deg. The thickness of the Intralipid layer was 125 μm. All the spectra were acquired as described in Sec. 2.3 and were later normalized to unity. The spectral regions where the specific signature of the epoxy-based phantom is visible—namely, around 1190 nm, 1140 nm, and 1721 nm—are marked with dotted lines and arrows.

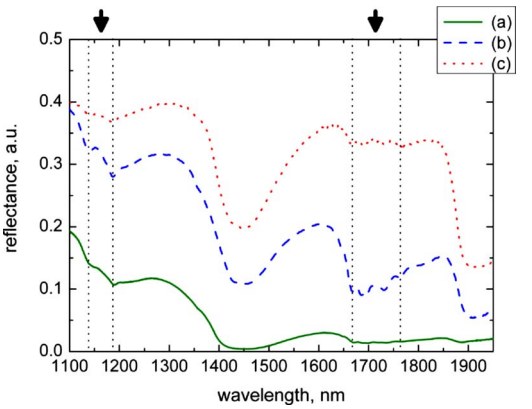

Fig. 5 Comparison of the diffuse back-reflectance spectra of a two-layer phantom acquired using (a) perpendicular-oriented fibers; (b) 20 deg inward tilt of the illumination fiber; and (c) 20 deg tilt of both illumination and detection fibers. The thickness of the Intralipid layer was 125 μm. All the spectra were acquired as described in Sec. 2.3 were later normalized to unity. The spectral regions where the specific signature of the epoxy-based phantom is visible—namely, around 1190 nm, 1140 nm, and 1721 nm—are marked with dotted lines and arrows.

of approximately 700 nm were used as input. Consequently, the very sharp spectral features of the epoxy-based phantom, although visible in the simulated spectra, are less distinctive than those featured in the original data sets (see Fig. 3).

4 Results and Discussion

4.1 *Experimental Data*

The aim of the first experiment was to demonstrate the dependency of the diffuse back-reflectance spectra on the angle of orientation of the illuminating fiber. In this experiment, the thickness of the Intralipid film positioned above the solid epoxy-based phantom was equal to 125 μm. As mentioned earlier, the optical properties, namely—the absorption coefficient—of this two-layer phantom are layer dependent, which can be observed in the corresponding spectra (see Fig. 3).

The expectation was that an increase in the angle would result in the probing of a more shallow volume and therefore (1) an increase in the overall reflectance, (2) an increase in the signal at the position of the highest absorption bands, and (3) a decrease in the contribution from the epoxy phantom.

As is revealed by the spectra [see Figs. 4(a)–4(d)], it is indeed the case that overall reflectance increases with increasing angle. This is conclusive with the confinement of light to more superficial layers.

It is also shown that an increase in angle results in a decrease in water absorption, which can be observed as a decrease in absorption around 1200 nm and reduced saturation of the detector around 1439 nm and 1920 nm.

Second, the increase in angle results in first increased and, later, decreased definition of the spectral features of the phantom around 1200 nm and 1700 nm [compare Figs. 4(b) and 4(c) versus 4(d), respectively]. This is because an increase in the angle of the illumination fiber results in a decrease in saturation of the detector caused by high absorption in the epoxy-based layer, thus revealing sharply the spectral features of the phantom. As the angle of the fiber increases further, the detected light is confined to the superficial layer (i.e., Intralipid), resulting in less pronounced absorption features of the epoxy layer.

In a second investigation, the effect of varying the angle of orientation of both fibers was compared with varying the orientation of only the illumination fiber, again with a fixed fiber-to-fiber separation distance of 820 μm and Intralipid sample thickness of 125 μm. The obtained spectra can be seen in Fig. 5. The expectation here was a more pronounced effect than that obtained in the case of only a single obliquely oriented fiber.

An important difference is observed when comparing traces (b) and (c), when either one [trace (b)] or both [trace (c)] fibers are oriented at an angle of 20 deg. There is more reflectance in the case when both fibers are oriented obliquely and less saturation of the signal at the 1439 nm and 1920 nm water band than in the case of the single obliquely oriented fiber. Furthermore, the contribution of the epoxy phantom is further decreased compared to the situation described by trace (a). This confirms our hypothesis that by obliquely orienting two fibers simultaneously, even greater depth selectivity can be achieved, i.e., the spectral features of more superficial layers can be measured in absence of (or with reduced interference from) deeper layers. The results of this experiment indicate the advantages of a dual obliquely oriented fiber arrangement, as opposed to a singular obliquely oriented fiber, such as described in Ref. 15.

In a third experiment, we compared an obliquely oriented fiber pair, set at an angle of 25 deg *outward*, with a dual perpendicular arrangement [see Fig. 1(b)]. The aim was to compare the effect of directing the light into the sample such that the light cones did not overlap or deliberately confine light to shallow layers. It was previously postulated that this could result in a deeper overall penetration capability, with better-defined spectral features of the deeper layers of the

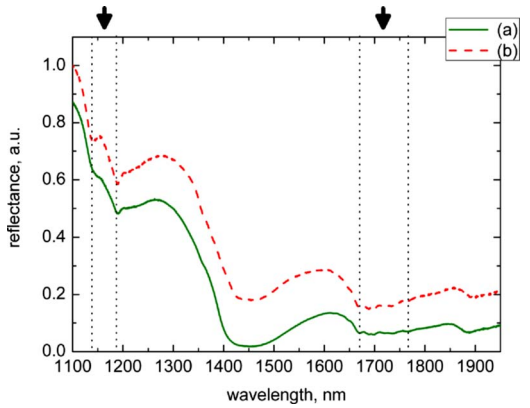

Fig. 6 Comparison of the diffuse back-reflectance spectra of a two-layer phantom acquired using (a) perpendicular-oriented fibers; and (b) 25 deg outward tilt of both illumination and detection fibers. The thickness of the Intralipid layer was 125 μm. All the spectra were acquired as described in Sec. 2.3 and normalized to unity. The graphs are shifted along the *y* axis for clarity. The spectral regions where the specific signature of the epoxy-based phantom is visible—namely, around 1190 nm, 1140 nm, and 1721 nm—are marked with dotted lines and arrows.

sample due to the reduction of interference from the more superficial layers.[15]

In Fig. 6, the results of a perpendicular arrangement [trace (a)] can be seen plotted against the outwardly obliquely oriented fiber pair [trace (b)]. The significance of the result is in the degree of selectivity in probing depth by only obliquely orienting the fibers: in the case of the dual perpendicular arrangement, a more superficial layer is probed, which is observed as a dominant contribution of Intralipid with little contribution of the epoxy phantom below. In the case of dual outward orientation, a deeper layer, i.e., the epoxy phantom, is probed (seen as an increase in the sharp, phantom-specific spectral features around 1200 nm). This effect is visible only in spectral regions having a low absorption coefficient (e.g., around 1200 nm) because outside of these regions, the photons are already being absorbed in more superficial layers. Note that the data was normalized to unity and shifted such that it could be displayed clearly and without overlapping.

4.2 *Monte Carlo Simulations*

4.2.1 *Dependence of the mean penetration depth and variation thereof on fiber angle*

The results of the Monte Carlo simulations were used to calculate the mean penetration depth, the variation in the mean penetration depth, and the number of scattering events of the detected photons for the two-layer phantom, as a function of fiber angle and wavelength.

The resulting spectra and the corresponding estimated parameters are given in Table 1 and Figs. 7 and 8, respectively. The data presented in Table 1 demonstrate the following trends:

- As the inward tilt of an illumination fiber increases, the maximal penetration depth, the mean penetration depth, and the spread in the penetration decrease (see Table 1).
- With an increase in the inward tilt of an illumination fiber, the distribution of the number of the scattering events of the detected photons is shifted toward lower values (see Fig. 8).
- For a large fiber angle of 60 deg, the mean penetration depth is restricted to the Intralipid layer, i.e., to 125 μm at

Table 1 Comparison of the mean penetration depths and the variation in the mean penetration depth [see Eqs. (1) and (2)] for the two-layer tissue-mimicking phantom as obtained using Monte Carlo simulations for different fiber angles and different wavelengths. Inward and outward fiber tilt is noted as positive and negative angles, respectively. The thickness of the Intralipid layer was constant and equal to 125 μm.

Angle (deg)	Mean penetration depth (μm)	Variation in penetration depth (μm)
	1187 nm	
0	533	340
20	374	308
40	317	275
60	191	219
−10	526	410
−25	540	386
−50	538	462
	1459 nm	
0	415	320
20	283	275
40	221	203
60	100	148
−10	428	347
−25	456	396
−50	432	386
	1697 nm	
0	422	283
20	302	259
40	268	212
60	145	148
−10	457	319
−25	456	323
−50	451	332
−10	520	398
−25	538	418
−50	577	493

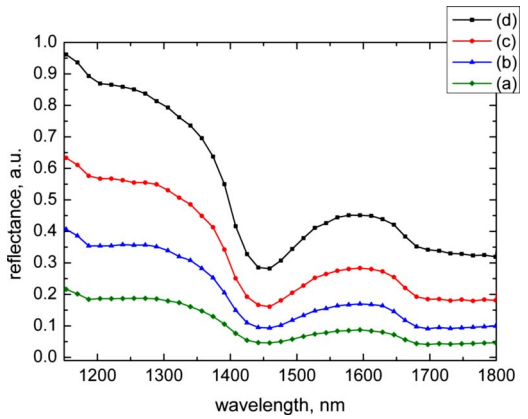

Fig. 7 Dependence of diffuse back-reflectance spectra of a two-layer phantom on the inward tilt of the illumination fiber, which was (a) 0 deg; (b) 20 deg; (c) 40 deg; and (d) 60 deg. The spectra were obtained using Monte Carlo simulation. The thickness of the Intralipid layer was 125 μm. The data were normalized to unity.

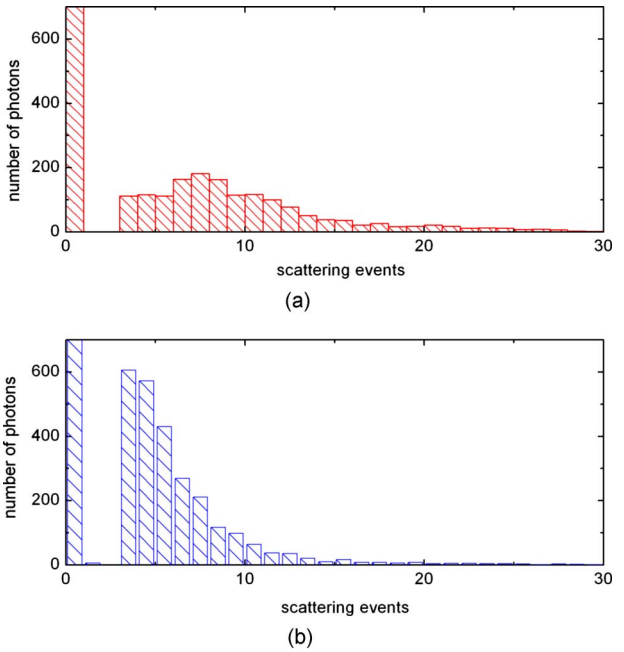

Fig. 8 The number of photon scattering events in the two-layer phantom for (a) perpendicular-oriented fibers; and (b) 60 deg inward orientation of the illumination fiber. The data were obtained by analyzing the photon tracks resulting from the Monte Carlo simulation at 1459-nm wavelength. Note that unscattered photons result from reflectance at the interface between glass and immersion fluid (see Fig. 1).

1459 nm, with minor penetration into the epoxy phantom at 1187 nm and 1697 nm (see Table 1).

• An increase in the inward angle of the illumination fiber results in a decrease in the variation of the penetration depth—for example, for a 60 deg inward angle, we observed an approximately twofold decrease in the variation of the penetration depth when compared to an angle of 0 deg (see Table 1).

Thus, the general results of these simulations support the assumption made earlier—namely, that by varying the angle of orientation of a fiber, the depth to which a sample is probed can be varied accordingly. Moreover, an increase in inward angle of an illumination fiber also results in a decrease in a variation of the penetration depth. The changes in light interaction with the sample when using an obliquely oriented illumination fiber are also characterized by a decreased number of scattering events, as shown in Fig. 8.

The spectral data obtained using Monte Carlo simulations (see Fig. 7), qualitatively support our experimental results presented in Sec. 4.1 (see Fig. 4). Namely, (1) as the fiber angle increases, the contributions of both water and epoxy phantom in the spectrum decrease, (2) the total amount of light back-reflected from the sample increases, and (3) there is no significant contribution of the epoxy phantom visible in the spectrum at 60 deg fiber angle [see Figs. 4(d) and 7(d)], which manifests as a diminished epoxy-specific spectral signature at 1200 nm and its total absence at around 1700 nm. In order to better distinguish the differences in contribution as separate components, a more rigorous analysis can be performed such as the chemometric techniques employed by Pham et al. and Berger et al.[26,27]

4.2.2 *Comparison of a variable-angle oblique arrangement with a variable-distance perpendicular arrangement*

Our next step was to test whether the effect of using an inward oblique arrangement could be approximated to a decrease in fiber-to-fiber separation distance in the case of a perpendicular fiber arrangement. Our approach was to verify that the spectral intensity for the obliquely oriented arrangement could be matched to that of the perpendicular arrangement. In particular, the aim was to determine the fiber-to-fiber separation distance required in the perpendicular arrangement for match in light intensity (outside strong absorption bands) with a single obliquely oriented arrangement at a fixed fiber-to-fiber separation distance.

For this purpose, we used Monte Carlo simulations to simulate the spectral response of a single-layer Intralipid-based phantom of 5 mm thickness. The calculations were performed for a fiber diameter of 100 μm. The former was done to simplify the shape of the spectral response and as a result the interpretation thereof, while the latter decreased the spread in the photon paths.

In the first case, the illumination fiber was positioned at a fixed 500-μm distance with respect to the detection fiber, but at varying angles of 10, 20, 30, 40, 50, and 60 deg. In the second case, two perpendicular fibers were used at varying distances.

Figure 9 shows an example of the spectrum: the intensity obtained using an inward obliquely oriented arrangement at an angle of 60 deg and fiber-to-fiber separation distance of 500 μm is matched (outside of strong absorption bands) to the intensity obtained by using a perpendicular oriented arrangement with a fiber-to-fiber separation distance of 200 μm.

For all other cases, the required fiber-to-fiber separation for the perpendicular arrangement, which gives the same spectral intensity as an obliquely oriented fiber arrangement at fixed separation distance, is shown in Table 2. Note that the corre-

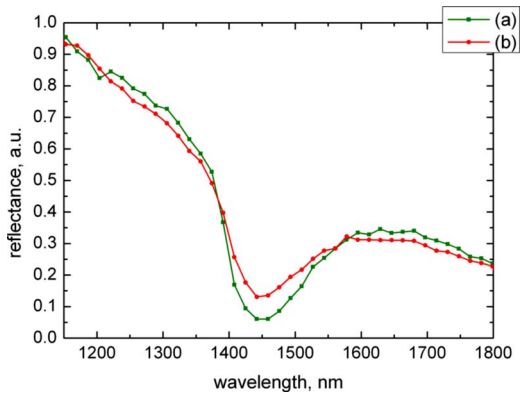

Fig. 9 Comparison of the diffuse back-reflectance spectra of a homogeneous Intralipid-based phantom obtained using (a) an obliquely oriented arrangement at 60-deg inward tilt with 500-micrometer fiber-to-fiber distance and (b) a perpendicular arrangement with 200-micrometer fiber-to-fiber distance. The spectra were obtained using Monte Carlo simulation. 100-micrometer-diameter fibers were used in this simulation. The data were normalized to unity.

Table 2 Comparison of the fiber-to-fiber separation distances for the oblique arrangement at varying inward tilt and the perpendicular arrangement and varying fiber-to-fiber distance.

Inward tilt (deg)	Fiber-to-fiber distance for oblique arrangement (μm)	Fiber-to-fiber distance for perpendicular arrangement (μm)
60	500	200
50	500	220
40	500	260
30	500	310
20	500	360
10	500	550

spondence between an inward tilt of the fiber and the shift in the separation distance between the perpendicular fibers is calculated for the given scattering and absorption coefficient of the sample as well as for the given refractive indices of the sample and surrounding medium. Yet, in general, the required decrease in the fiber-to-fiber distance in the case of a perpendicular arrangement will follow a cosine law with respect to the angle corresponding to the inward tilt, as supported by the data shown in Table 2.

The corresponding mean penetration depths at the wavelengths outside as well as within the strong absorption band (1136-nm and 1459-nm wavelengths, respectively) are given in Table 3.

The data presented in Fig. 9 and Table 2 confirm that indeed the effect of using an inward oblique arrangement can be approximated to a decrease in fiber-to-fiber separation distance in the case of a perpendicular fiber arrangement. Note that a significant reduction of fiber-to-fiber separation between perpendicular fibers is required to achieve the same intensity as yielded when using a single obliquely oriented arrangement.

Furthermore, although this approximation is valid in the regime of weak or no absorption ($\mu_a \ll \mu_s'$), it does not hold completely for the regions of high absorption. This observation is based on the data presented in Fig. 9 and Table 3. Namely, as can be seen in Fig. 9, while outside the strong absorption band there is an intensity match between the spectra obtained using an obliquely and perpendicular oriented fiber arrangement, no such match is observed at the position of the strong absorption band, i.e., around 1440 nm. In particular, absorption was slightly higher for the case of the oblique arrangement. This mismatch in the intensity was highest for the largest angle of the inward tilt (in our case, 60 deg) and decreased with decreasing inward tilt. Table 3 shows the

Table 3 Comparison of the mean penetration depth outside and within the strong absorption band for the oblique arrangement at varying inward tilt and the perpendicular arrangement and varying fiber-to-fiber distance.

		Mean penetration			Mean penetration	
Inward tilt (deg)	Fiber-to-fiber distance for oblique arrangement (μm)	1136 nm	1459 nm	Fiber-to-fiber distance for perpendicular arrangement (μm)	1136 nm	1459 nm
60	500	265	109	200	262	88
50	500	285	109	220	283	89
40	500	291	112	260	308	93
30	500	338	115	310	321	97
20	500	365	116	360	351	103
10	500	367	112	550	334	110

mean penetration depths for the obliquely and perpendicularly oriented cases calculated both outside and within the strong absorption—namely, at 1136 nm and 1459 nm. It can be seen that the effect of using an inward oblique arrangement can indeed be approximated to a decrease in fiber-to-fiber separation distance, in the case of a perpendicular fiber arrangement—there is a good correspondence in mean penetration depth between the oblique and the perpendicular arrangements at 1136 nm, i.e., outside the strong absorption band. However, there is a mismatch between the calculated mean penetration depths corresponding to the 1459-nm wavelength. The penetration depth is larger for the inward oriented oblique configuration when compared to that of the perpendicular arrangement. This difference is more pronounced at larger angles, e.g., the corresponding difference is around 1% for the 10 deg angle and reaches 20% for angles of 50 and 60 deg. This increase in penetration depth corresponds to an increase in light absorption in the case of the oblique arrangement, as shown in Fig. 9. This effect can be accounted for as follows. First, by launching light into the sample under an oblique angle, the virtual isotropic point source, to which the beam can be approximated, is located closer to the surface. In other words, light is more confined to the superficial layers (see Ref. 2). The larger the angle, the more confined the light is to the surface of the sample. Therefore, to achieve an intensity match between an obliquely and a perpendicularly oriented arrangement, one needs to significantly decrease the fiber-to-fiber separation of the perpendicular-oriented fibers.

As a result, the larger fiber-to-fiber separation distance in the case of the inward obliquely oriented arrangement yields a longer average photon trajectory. This in turn increases the probability of an absorption event, which results in stronger light absorption within the absorption band (see Fig. 9).

5 Conclusions

To summarize, in this investigation, we demonstrated the effect of using obliquely positioned fibers on depth selectivity in near-infrared diffuse reflectance spectroscopy. Our experimental results combined with Monte Carlo simulations confirm that by using obliquely oriented fibers, significant improvement of depth selectivity can be achieved. This supports the benefit of using a dual obliquely oriented fiber configuration for improved selectivity in measurements.

We also demonstrated that a symmetrical arrangement of outwardly obliquely oriented fibers can yield light confinement to a volume at some depth within the superficial layers. This result is of particular importance if, for example, features within the dermis are to be studied without significant influence from the uppermost skin layers. This has not, to our awareness, been previously demonstrated in the literature.

Additionally, we have compared an obliquely oriented arrangement at a fixed fiber-to-fiber distance with a perpendicularly oriented arrangement at varying fiber-to-fiber separation. The results support a statement that the effect of using an inward oblique arrangement can be approximated to a decrease in fiber-to-fiber separation distance in the case of a perpendicular fiber arrangement outside strong absorption bands.

These results assert the advantages of using obliquely oriented fibers in near-infrared diffuse reflectance when attempting to specifically address superficial tissue layers, for example, at depths of up to 100 μm for skin cancer detection, or selectively probing the deeper layers at 300 μm for noninvasive glucose monitoring. Such flexibility could be further advantageous in a range of minimally invasive or noninvasive applications, including catheter-based interventions.

References

1. B. C. Wilson, "Measurements of optical properties: methods and theories," in *Optical-Thermal Response of Laser-Irradiated Tissue*, A. J. Welch and M. J. C. van Gemert, Eds., pp. 223–303, Plenum Press, New York (1995).
2. L. Wang and S. L. Jacques, "Use of a laser beam with an oblique angle of incidence to measure the reduced scattering coefficient of a turbid medium," *Appl. Opt.* **34**(13), 2362–2366 (1995).
3. G. Marquez and L. V. Wang, "White light oblique incidence reflectometer for measuring absorption and reduced scattering spectra of tissue-like turbid media," *Opt. Express* **1**(13) 454–460 (1997).
4. S.-P. Lin, L. H. Wang, S. L. Jacques, and F. K. Tittel, "Measurement of tissue optical properties by the use of oblique-incidence optical fiber reflectometry," *Appl. Opt.* **36**(1), 136–143 (1997).
5. G. Marquez, L. H. Wang, S.-P. Lin, J. A. Schwartz, and S. L. Thomsen, "Anisotropy in the absorption and scattering spectra of chicken breast tissue," *Appl. Opt.* **37**(4), 798–804 (1998).
6. K. Takagi, H. Haneishi, N. Tsumura, and Y. Miyake, "Alternative oblique-incidence reflectometry for measuring tissue optical properties," *Opt. Rev.* **7**(2), 164–169 (2000).
7. T. F. Cooney, H. T. Skinner, and S. M. Angel, "Comparative study of some fiber-optic remote Raman probe designs. Part I: model for liquids and transparent solids," *Appl. Spectrosc.* **50**(7), 836–848 (1996).
8. T. F. Cooney, H. T. Skinner, and S. M. Angel, "Comparative study of some fiber-optic remote Raman probe designs. Part II: tests of some single-fiber, lensed, and flat- and bevel-tip multifiber probes," *Appl. Spectrosc.* **50**(7), 849–860 (1996).
9. M. G. Shim, B. C. Wilson, E. Marple, and M. Wach, "Study of fiber-optic probes for *in vivo* medical Raman spectroscopy," *Appl. Spectrosc.* **53**(6), 619–627 (1999).
10. U. Utzinger and R. R. Richards-Kortum, "Fiber optic probes for biomedical optical spectroscopy," *J. Biomed. Opt.* **8**(1), 121–147 (2003).
11. M. C. Skala, G. M. Palmer, C. F. Zhu, Q. Liu, K. M. Vrotsos, C. L. Marshek-Stone, A. Gendron-Fitzpatrick, and N. Ramanujam, "Investigation of fiber-optic probe designs for optical spectroscopic diagnosis of epithelial pre-cancers," *Lasers Surg. Med.* **34**(1), 25–38 (2004).
12. Q. Liu and N. Ramanujam, "Experimental proof of the feasibility of using an angled fiber-optic probe for depth-sensitive fluorescence spectroscopy of turbid media," *Opt. Lett.* **29**(17), 2034–2036 (2004).
13. T. J. Pfefer, A. Agrawal, and R. A. Drezek, "Oblique-incidence illumination and collection for depth selective fluorescence spectroscopy," *J. Biomed. Opt.* **10**(4), 044016 (2005).
14. D. Hattery, B. Hattery, V. Chernomordik, P. Smith, M. Loew, J. Mulshine, and A. Gandjbakhche, "Differential oblique angle spectroscopy of the oral epithelium," *J. Biomed. Opt.* **9**(5), 951–960 (2004).
15. A. M. J. Wang, J. E. Bender, J. Pfefer, U. Utzinger, and R. A. Drezek, "Depth-sensitive reflectance measurements using obliquely oriented fiber probes," *J. Biomed. Opt.* **10**(4), 044017 (2005).
16. M. Mehrubeoglu, N. Kehtarnavaz, G. Marquez, M. Duvic, and L. V. Wang, "Skin lesion classification using oblique-incidence diffuse reflectance spectroscopic imaging," *Appl. Opt.* **41**(1), 182–192 (2002).
17. A. Garcia-Uribe, N. Kehtarnavaz, G. Marquez, V. Prieto, M. Duvic, and L. H. V. Wang, "Skin cancer detection by spectroscopic oblique-incidence reflectometry: classification and physiological origins," *Appl. Opt.* **43**(13), 2643–2650 (2004).
18. C.-C. Yu, C. Lau, G. O'Donoghue, J. Mirkovic, S. McGee, L. Galindo, A. Elackattu, E. Stier, G. Grillone, K. Badizadegan, R. R. Dasari, and M. S. Feld, "Quantitative spectroscopic imaging for noninvasive early cancer detection," *Opt. Express* **16**(20), 16227–16239 (2008).
19. Z. Volynskaya, A. S. Haka, K. L. Bechtel, M. Fitzmaurice, R. Shenk, N. Wang, J. Nazemi, R. R. Dasari, and M. S. Feld, "Diagnosing breast cancer using diffuse reflectance spectroscopy and intrinsic fluorescence spectroscopy," *J. Biomed. Opt.* **13**(2), 024012-1–9 (2008).

20. M. K. Simick, R. Jong, B. Wilson, and L. Lilge, "Non-ionizing near-infrared radiation transillumination spectroscopy for breast tissue density and assessment of breast cancer risk," *J. Biomed. Opt.* **9**(4), 794–803 (2004).
21. S. Kukreti, A. Cerussi, B. Tromberg, and E. Gratton, "Intrinsic tumor biomarkers revealed by novel double-differential spectroscopic analysis of near-infrared spectra," *J. Biomed. Opt.* **12**(2), 1–3 (2007).
22. W. L. Chen, R. Liu, K. X. Xu, and R. K. K. Wang, "Influence of contact state on NIR diffuse reflectance spectroscopy *in vivo*," *J. Phys. D* **38**(15), 2691–2695 (2005).
23. S. A. Prahl, M. J. C. van Gemert, and A. J. Welsch, "Determining the optical properties of turbid media by using the adding-doubling method," *Appl. Opt.* **32**(4), 559–568 (1993).
24. S. J. Choquette, J. C. Travis, C. Zhu, and D. L. Duewer, "Wavenumber standards for near-infrared spectrometry," in *Handbook of Vibrational Spectroscopy*, J. M. Chalmers and P. R. Griffiths, Eds., pp. 899–905. John Wiley & Sons, Chichester, UK (2002).
25. S. A. Prahl, M. Keijzer, S. L. Jacques, and A. J. Welch, "A Monte Carlo model of light propagation in tissue," in: *Dosimetry of Laser Radiation in Medicine and Biology*, G. Mueller and D. Sliney, Eds., *Proc. SPIE* **5**, 102–111 (1989).
26. T. H. Pham, C. Eker, A. Durkin, B. J. Tromberg, and S. Andersson-Engels, "Quantifying the optical properties and chromophore concentrations of turbid media by chemometric analysis of hyperspectral diffuse reflectance data collected using a Fourier interferometric imaging system," *Appl. Spectrosc.* **55**(8), 1035–1045 (2001).
27. A. J. Berger, V. Venugopalan, A. J. Durkin, T. Pham, and B. J. Tromberg, "Chemometric analysis of frequency-domain photon migration data: quantitative measurements of optical properties and chromophore concentrations in multicomponent turbid media," *Appl. Opt.* **39**(10), 1659–1667 (2000).